



Supplement of

A two-channel, Thermal Dissociation Cavity-Ringdown Spectrometer for the detection of ambient NO₂, RO₂NO₂ and RONO₂

J. Thieser et al.

Correspondence to: J. N. Crowley (john.crowley@mpic.de)

The copyright of individual parts of the supplement might differ from the CC-BY 3.0 licence.

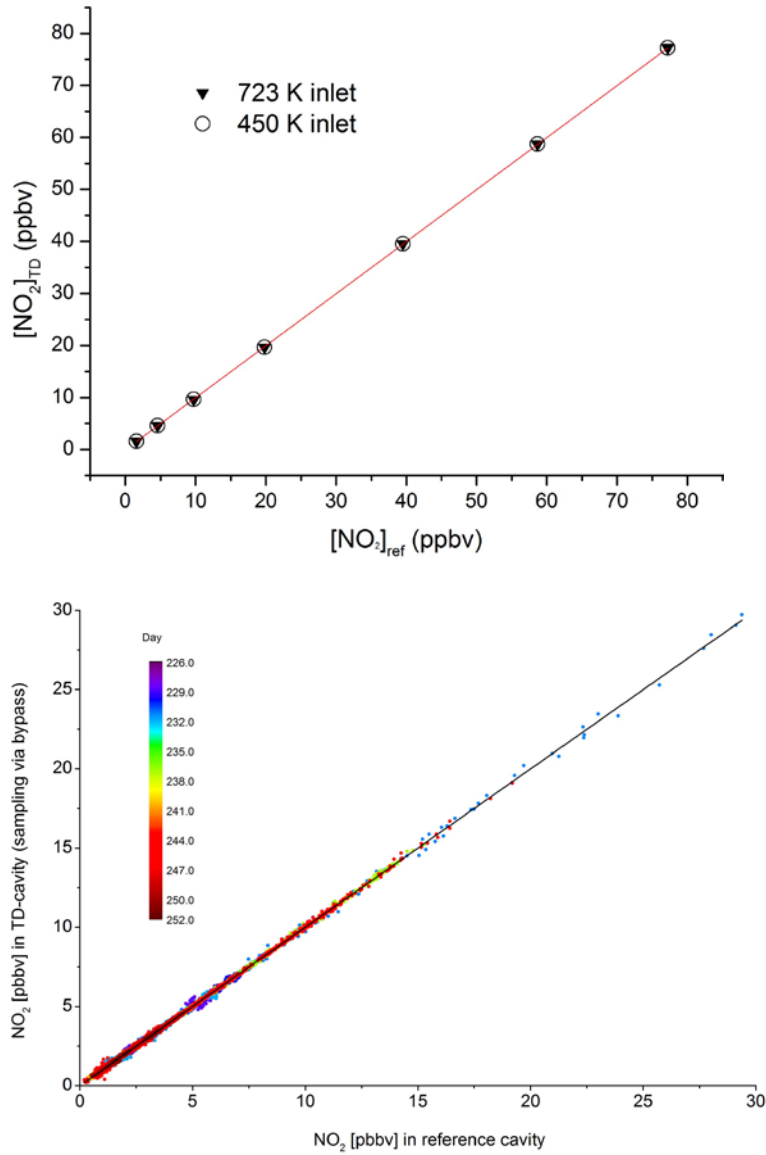


Figure SI 1 Upper panel: Comparison of response of the TD-cavity to additions of NO_2 . The reference cavity samples from the inlet at ambient temperature, the TD-cavity from inlets at either 450 or 723 K. The slope of the regression line is 1.000 ± 0.001 in both cases. Lower panel: Comparison of NO_2 mixing ratios obtained during the PARADE campaign using the reference cavity with those obtained when sampling via the non-heated bypass into the TD-cavity. The slope is 0.9997 ± 0.0002 . The colour code indicates that these measurements were taken over a period of 26 days, and the data covers $\sim 10\%$ of the entire instrument operation time.

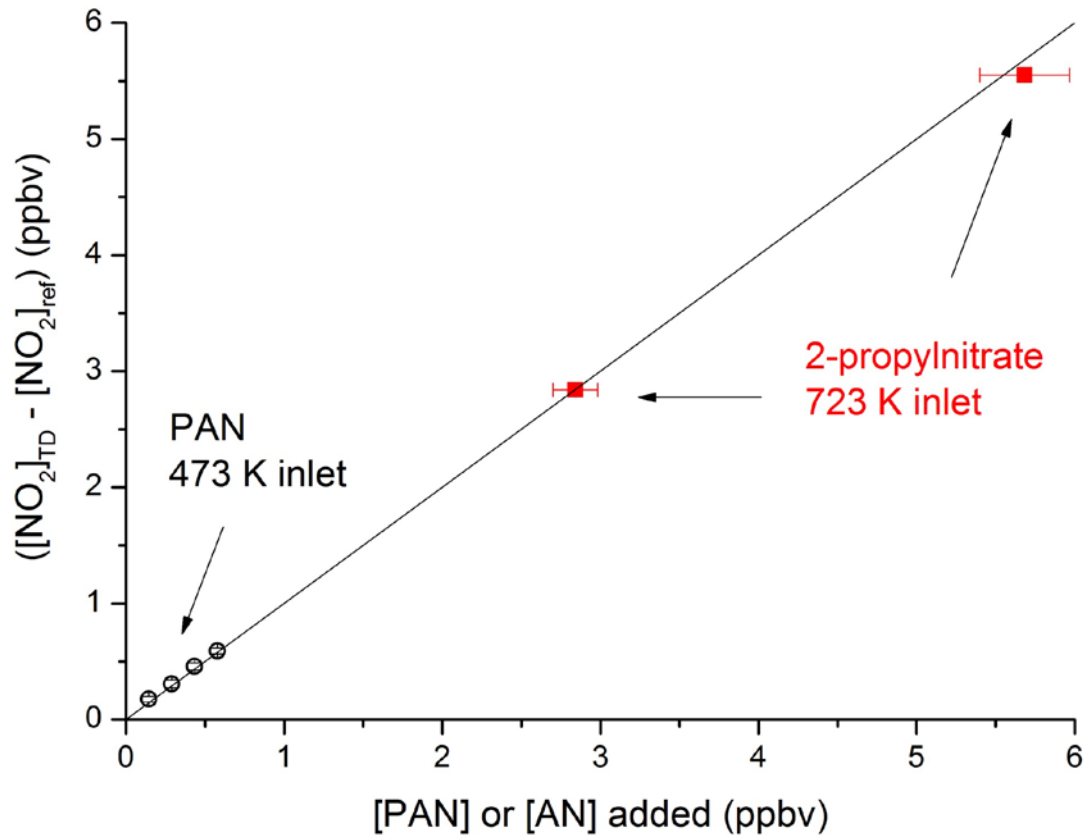


Figure SI 2. Addition (not simultaneous) of known amounts of PAN (black data points) and 2-propynitrate to the 473 K and 723 K inlets, respectively. The solid line represents the 1:1 conversion of both PAN and 2-propynitrate to NO₂.

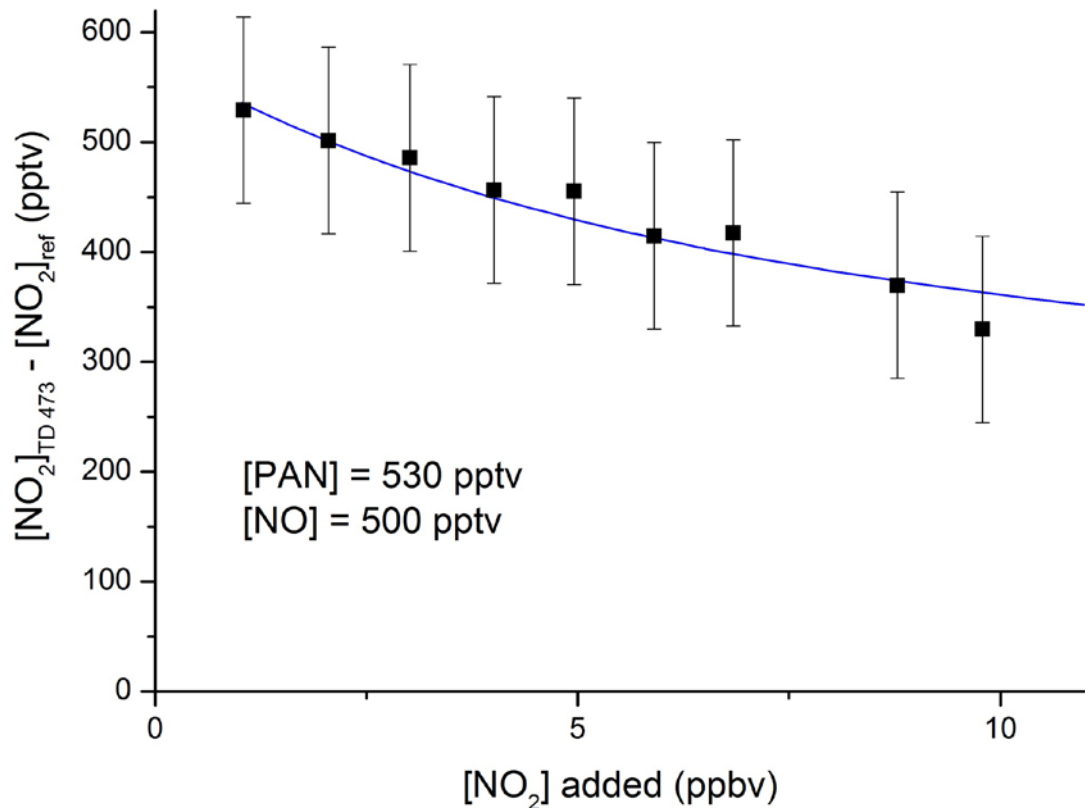


Figure SI 3. NO_2 formed in the TD channel at 473 K from adding various amounts of NO_2 (up to 10 ppbv) to 560 pptv PAN in presence of NO (500 pptv). The blue line is the model prediction.

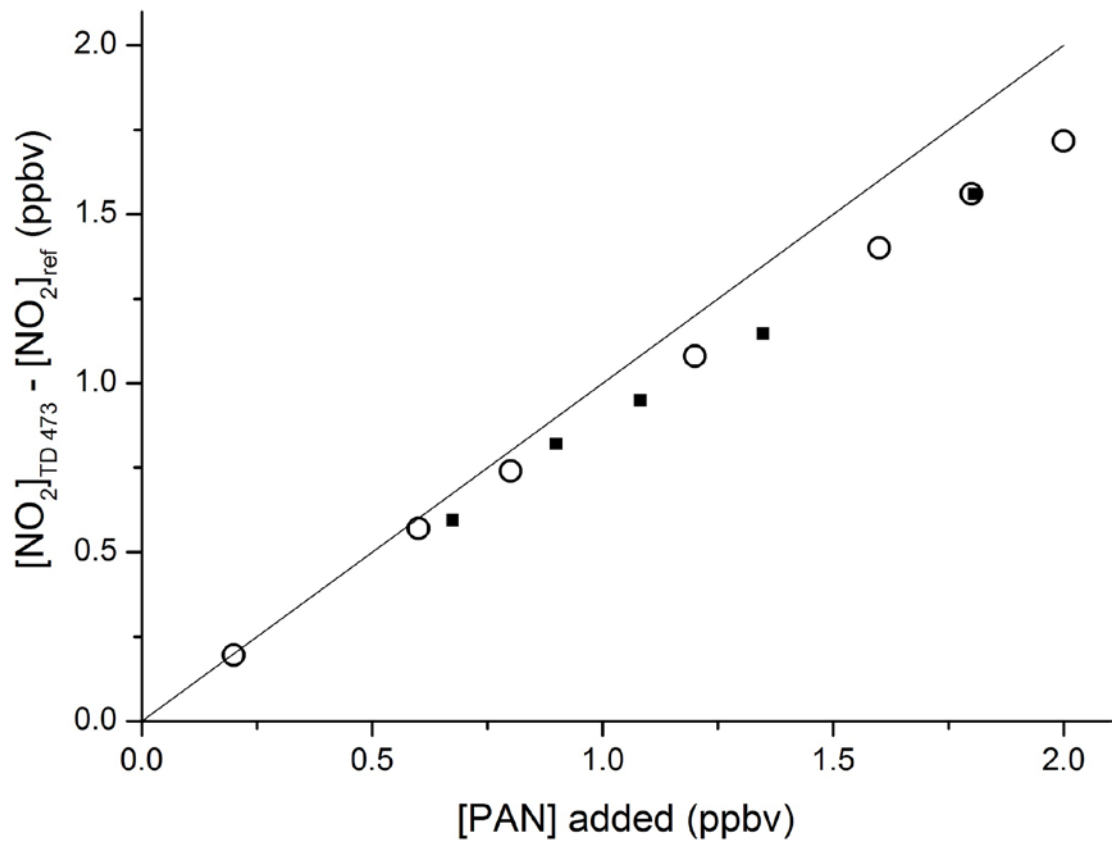


Figure SI 4 Measurement (solid squares) and modelling (open circles) of PAN generated in the photochemical PAN source. PAN added is calculated assuming 95 % conversion of NO. The open circles are the model prediction. The straight line represents 1:1 conversion of PAN to NO₂. The observed deviation from the straight is reproduced by the model, and confirming the results of the experiments in which NO and NO₂ were added.

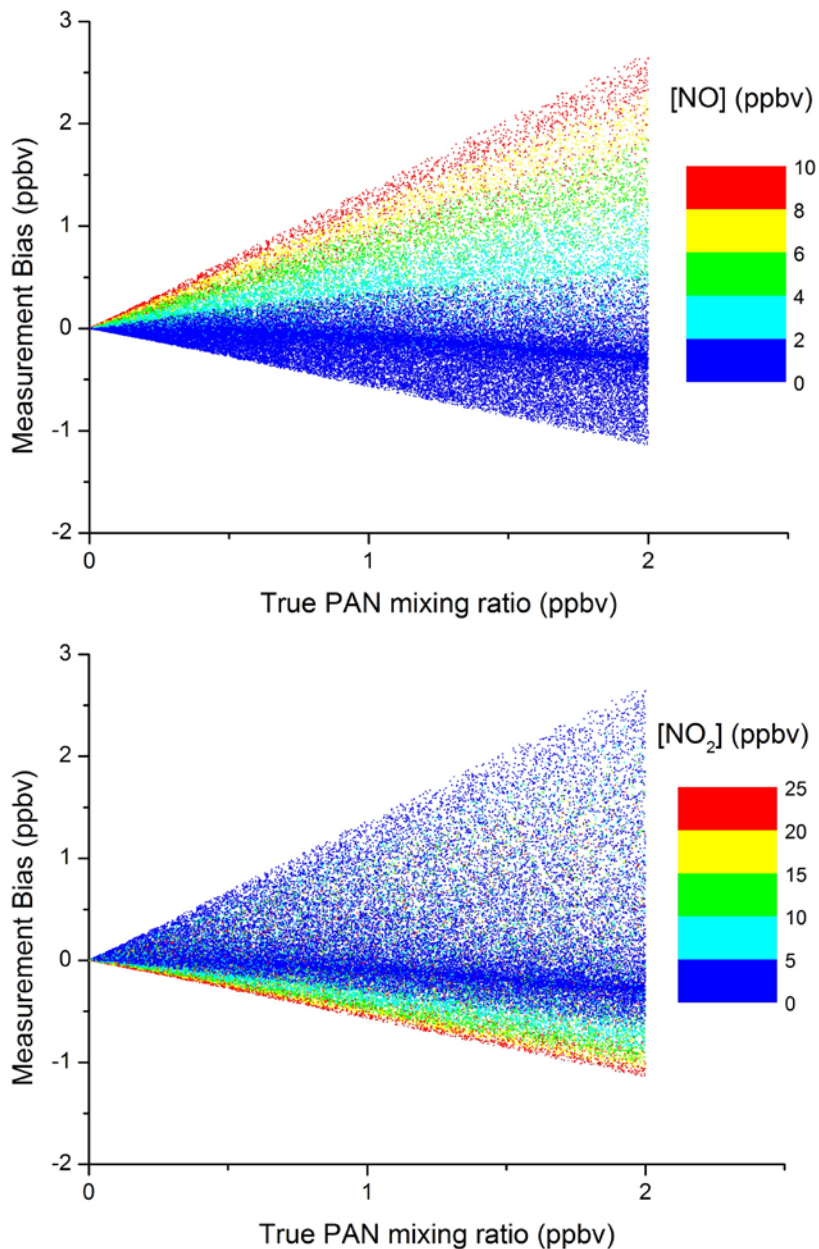


Figure SI 5. Result of ~90000 simulations of the inlet / cavity chemistry initiated with various NO, NO_2 and PAN concentrations, the range of which was selected to cover the values observed at the PARADE field campaign. A large measurement positive bias is associated with high NO or low NO_2 and vice-versa.

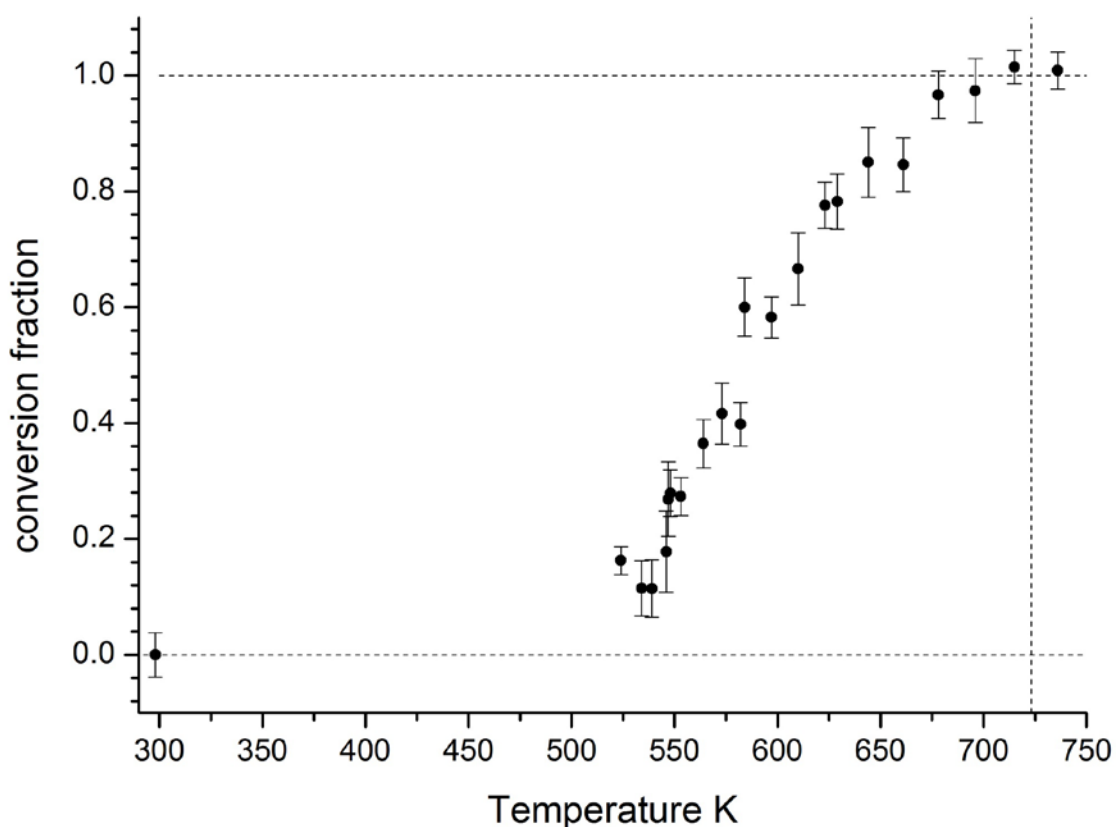


Figure SI 6. Thermal decomposition of ClNO_2 in the 723 K inlet. The horizontal, dashed lines indicate the 0 and 100 % conversion efficiencies. The vertical dashed lines indicates the temeprature at which the inlet was operated (723 K) when measuring ΣANs .

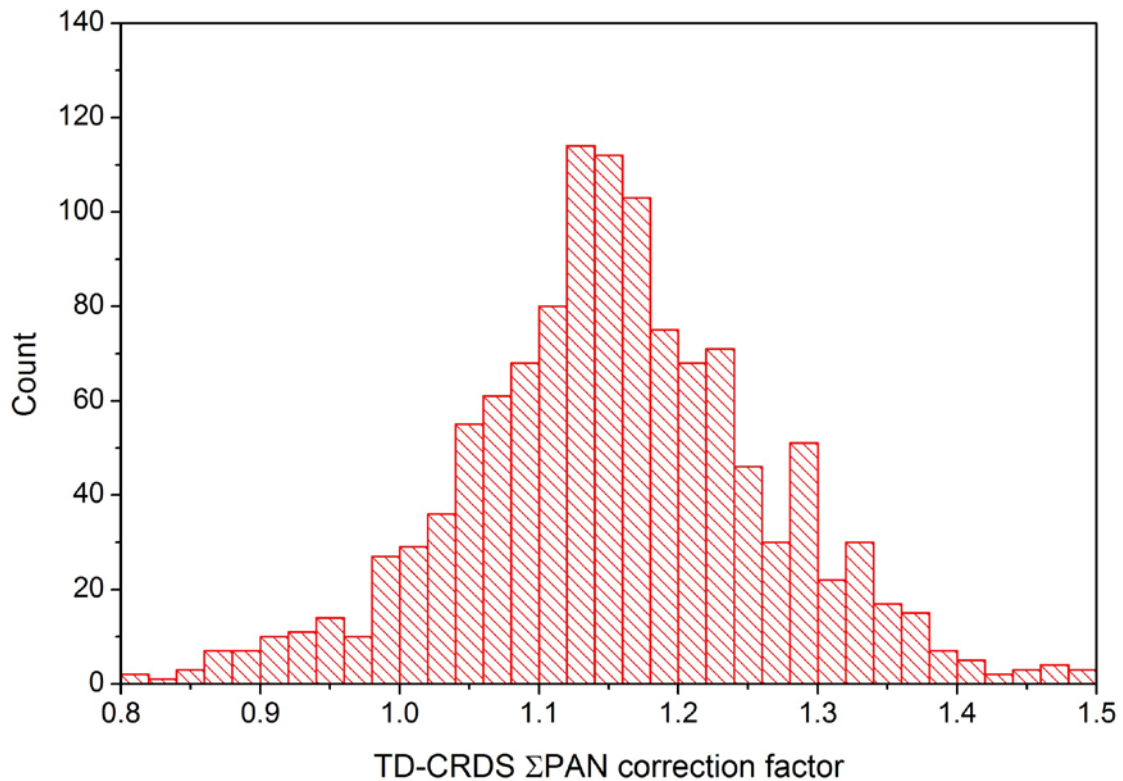


Figure SI 7. Frequency distribution of the simulation derived correction factors for the TD-CRDS measurements of Σ PANs during the PARADE campaign.

1 **Chemical scheme used in the numerical simulations.**

2

3 k1 : PAN = CH₃CO₃ + NO₂
4 k2 : CH₃CO₃ + NO₂ = PAN
5 k3 : CH₃CO₃ + NO = CH₃CO₂ + NO₂
6 k3a : CH₃CO₂ = CH₃O₂ + CO₂
7 k4 : CH₃O₂ + NO = HCHO + HO₂ + NO₂
8 k5 : CH₃O₂ + NO₂ = CH₃O₂NO₂
9 k6 : CH₃O₂NO₂ = CH₃O₂ + NO₂
10 k7 : HO₂ + NO = NO₂ + OH
11 k8 : HO₂ + NO₂ = HO₂NO₂
12 k9 : HO₂NO₂ = HO₂ + NO₂
13 k10 : OH + NO₂ = HNO₃
14 k11 : OH + NO = HONO
15 k12 : CH₃CO₃ + CH₃CO₃ = CH₃CO₂ + CH₃CO₂
16 k13 : CH₃CO₃ + CH₃O₂ = HCHO + HO₂ + CH₃O₂ + CO₂
17 k14*0.29 : CH₃CO₃ + HO₂ = PAA + O₂
18 k14*0.1 : CH₃CO₃ + HO₂ = AA + O₃
19 k14*0.61 : CH₃CO₃ + HO₂ = OH + CH₃O₂
20 k15 : CH₃O₂ + HO₂ = CH₃OOH
21 k16 : HO₂ + HO₂ = H₂O₂
22 k17 : OH + HO₂ = H₂O + O₂
23 k18 : IPN = IPO + NO₂
24 k19 : IPO + O₂ = HO₂ + acetone
25 k19a : IPO + O₂ = CH₃O₂ + CH₃CHO
26 k26 : OH + CH₃CHO = CH₃CO
27 k20 : CH₃CO₃ = CH₃CO
28 k21 : CH₃CO₃ = CH₂COOOH
29 k23 : CH₂COOOH = CH₂CO₂ + OH
30 k24 : CH₃CO + O₂ = CH₃CO₃
31 k24a : CH₃CO + O₂ = OH + CH₂CO₂
32 k25 : CH₃CO = CH₃O₂
33 k26 : OH + CH₃O₂ = HO₂ + HO₂
34 k27 : OH + CH₃CO₃ = HO₂ + CH₃O₂ + CO₂
35

36 Note that the reactions are not numbered the same as in the manuscript
37 IPN = 2-propyl nitrate
38 IPO = C₃H₇O

39

40

41 k1 = ((1.10e-5*exp(-10100/T))*M*
42 (1.9e17*exp(-14100/T)))/((1.10e-5*exp(-10100/T))*M+
43 (1.9e17*exp(-14100/T)))*10^(log10(0.3)/
44 (1+(log10((1.10e-5*exp(-10100/T))*M/
45 (1.9e17*exp(-14100/T)))/(0.75-1.27*log10(0.3)))^2))

46

47 k2 = ((3.28e-28*(T/300)^-6.87)*M*
48 (1.125e-11*(T/300)^-1.105))/((3.28e-28*(T/300)^-6.87)*M+
49 (1.125e-11*(T/300)^-1.105))*10^(log10(0.3)/
50 (1+(log10((3.28e-28*(T/300)^-6.87)*M/
51 (1.125e-11*(T/300)^-1.105))/(0.75-1.27*log10(0.3)))^2))

52

53 k3 = 7.5e-12*exp(290/T)

54

55 k3a = 1e6

```

1 k4 = 2.3e-12*exp(360/T)
2
3 k5 = ((2.5e-30*(T/300)^-5.5)*M*
4 (1.8e-11))/((2.5e-30*(T/300)^-5.5)*M+
5 (1.8e-11))*10^(log10(0.36)/(1+(log10((2.5e-30*(T/300)^-5.5)
6 *M/(1.8e-11))/(0.75-1.27*log10(0.36))))^2))
7
8 k6 = ((9e-5*exp(-9690/T))*M*
9 (1.1e16*exp(-10560/T)))/((9e-5*exp(-9690/T))*M+
10 (1.1e16*exp(-10560/T)))*10^(log10(0.36)/
11 (1+(log10((9e-5*exp(-9690/T))*M/
12 (1.1e16*exp(-10560/T))))/(0.75-1.27*log10(0.36))))^2))
13
14 k7 = 3.45e-12*exp(270/T)
15
16 k8 = ((1.4e-31*(T/300)^-3.1)*M*
17 (4.0e-12))/((1.4e-31*(T/300)^-3.1)*M+
18 (4.0e-12))*10^(log10(0.4)/(1+(log10((1.4e-31*(T/300)^-3.1)
19 *M/(4.0e-12))/(0.75-1.27*log10(0.4))))^2))
20
21 k9 = (4.1e-5*exp(-10650/T))*M*
22 (6.0e15*exp(-11170/T))/((4.1e-5*exp(-10650/T))*M+
23 (6.0e15*exp(-11170/T)))*10^(log10(0.4)/
24 (1+(log10((4.1e-5*exp(-10650/T))*M/
25 (6.0e15*exp(-11170/T))))/(0.75-1.27*log10(0.4))))^2))
26
27 k10 = ((3.2e-30*(T/300)^-4.5)*M*
28 (3.0e-11))/((3.2e-30*(T/300)^-4.5)*M+
29 (3.0e-11))*10^(log10(0.41)/(1+(log10((3.2e-30*(T/300)^-4.5)
30 *M/(3.0e-11))/(0.75-1.27*log10(0.41))))^2))
31
32 k11 = ((7.4e-31*(T/300)^-2.4)*M*
33 (3.3e-11*(T/300)^-0.3))/((7.4e-31*(T/300)^-2.4)*M+
34 (3.3e-11*(T/300)^-0.3))*10^(log10(0.81)/
35 (1+(log10((7.4e-31*(T/300)^-2.4)*M/
36 (3.3e-11*(T/300)^-0.3))/(0.75-1.27*log10(0.81))))^2))
37
38 k12 = 2.9e-12*exp(500/T)
39
40 k13 = 2.0e-12*exp(500/T)
41
42 k14 = 7.6e-13*exp(980/T)
43
44 k15 = 3.8e-13*exp(780/T)
45
46 k16 = (2.2e-13*exp(600/T) + 1.9e-33*M*exp(980/T))
47
48 k17 = 4.8e-11*exp(250/T)
49
50 k18 = 3.16e16*exp(-20129/T)
51
52 k19 = 1.9e-14*exp(-300/T)
53
54 k19a = 5.33e19*T^-1.7*exp(-8630/T)
55
56 k20 = 1.5e16*exp(-20000/T)
57

```

```

1 k21 = (0.20) * 1.6e16*exp(-20000/T)
2 k23 = 1.8e18*exp(-20000/T)
3
4 k24 = (HPL24*LPL24*M/(LPL24*M+HPL24))*  

5 0.8^( (1+(log10(LPL24*M/HPL24))^2)^-1 )
6 LPL24 = 7.39e-30*(T/300)^-2.2
7 HPL24 = 4.88e-12*(T/300)^-0.85
8
9 k24a = kint*(1-k24/HPL24)
10 kint = 6.4e-14*exp(820/T)
11
12
13
14
15 k25 =((1.0e-8*exp(-7080/T))*M*  

16 (2.0e13*exp(-8630/T)))/((1.0e-8*exp(-7080/T))*M+  

17 (2.0e13*exp(-8630/T)))*10^(log10(0.5)/(1+(log10(  

18 (1.0e-8 *exp(-7080/T))*M/(2.0e13*exp(-8630/T)))/  

19 (0.75-1.27*log10(0.5)))^2))
20
21 k26 = k27 = 2e-10
22
23

24 Rate coefficients were taken from IUPAC where available: (IUPAC, 2015)
25 Exceptions are:
26 k3a Chosen to be essentially instantaneous
27 k14 Rate coefficient and branching ratio for OH formation from (Groß et al., 2014)
28 k18 2-propyl nitrate thermal decomposition rate constant from (Day et al., 2002)
29 k20-24 See text in manuscript.
30 k25 (Baulch et al., 2005)
31 k26, k27 ~collision rate (Bossolasco et al., 2014; Farago et al., 2015)
32
33
34
35
36
37
38
39

```

1 **References**

2

3 Baulch, D. L., Bowman, C. T., Cobos, C. J., Cox, R. A., Just, T., Kerr, J. A., Pilling, M. J.,
4 Stocker, D., Troe, J., Tsang, W., Walker, R. W., and Warnatz, J.: Evaluated kinetic data for
5 combustion modeling: Supplement II, *J. Phys. Chem. Ref. Data*, 34, 757-1397, 2005.

6 Bossolasco, A., Farago, E. P., Schoemaecker, C., and Fittschen, C.: Rate constant of the
7 reaction between CH₃O₂ and OH radicals, *Chem. Phys. Lett.*, 593, 7-13,
8 10.1016/j.cplett.2013.12.052, 2014.

9 Day, D. A., Wooldridge, P. J., Dillon, M. B., Thornton, J. A., and Cohen, R. C.: A thermal
10 dissociation laser-induced fluorescence instrument for in situ detection of NO₂, peroxy
11 nitrates, alkyl nitrates, and HNO₃, *J. Geophys. Res.*, 107, 4046-, 2002.

12 Farago, E. P., Schoemaecker, C., Viskolcz, B., and Fittschen, C.: Experimental determination
13 of the rate constant of the reaction between C₂H₅O₂ and OH radicals, *Chem. Phys. Lett.*,
14 619, 196-200, 10.1016/j.cplett.2014.11.069, 2015.

15 Groß, C. B. M., Dillon, T. J., Schuster, G., Lelieveld, J., and Crowley, J. N.: Direct Kinetic
16 Study of OH and O₃ Formation in the Reaction of CH₃C(O)O₂ with HO₂, *The Journal of
17 Physical Chemistry A*, 118, 974-985, 10.1021/jp412380z, 2014.

18 IUPAC: Task Group on Atmospheric Chemical Kinetic Data Evaluation, (Ammann, M., Cox,
19 R.A., Crowley, J.N., Jenkin, M.E., Mellouki, A., Rossi, M. J., Troe, J. and Wallington, T. J.)
20 <http://iupac.pole-ether.fr/index.html>, 2015.

21

22